Structure Formation at the Interface of Liquid/Liquid Bilayer in Electric Field

Zhiqun Lin, Tobias Kerle,† and Thomas P. Russell*

Department of Polymer Science and Engineering, University of Massachusetts at Amherst, Amherst, Massachusetts 01003

Erik Schäffer and Ullrich Steiner

Department of Polymer Chemistry, University of Groningen, Groningen, The Netherlands

Received December 26, 2001

ABSTRACT: Subjecting a liquid/liquid interface to an electrohydrodynamic pressure enhances fluctuations with a characteristic wavelength leading to an instability and the formation of well-defined columnar structures. An extension of a linear stability analysis for a single fluid interface to the bilayer case produced general arguments applicable to any interface. Countering the electrohydrodynamic pressure is the Laplace pressure, which for films is dictated by the surface energy; whereas for a bilayer, it is given in terms of the interfacial energy. Consequently, the characteristic length scale is reduced in the case of bilayers. Results are presented for different polymer bilayers under a wide range of experimental conditions showing quantitative agreement with the generalized theory with no adjustable parameters. Over 4 orders of magnitude in reduced wavelength and field strength can be described by these arguments. These results point to a viable route by which structures can be produced over a wide range of length scales.

Introduction

The influence of an electrical field on the surface of a polymer or viscous fluid was first investigated by Swan in 1897.[1] In conjunction with the development of xerography, Glenn described a process called "thermoplastic recording", for recording electrical signals that involved focusing an electron beam on low melting thermoplastics films.[2] Cressman subsequently developed a one-dimensional model to describe instabilities on the surface of a thin, thermoplastic film between two electorodes after placing a uniform charge on the surface.[3] Killat extended these studies to thicker films under the influence of a surface charge that led to a deformation of the thermoplastic.[4] Using low viscosity fluids, Reynolds investigated the interface between two fluids under an alternating field where the influence of surface charge is minimized.[5] These studies indicated that the interface would be unstable when the applied field exceeded a critical value. Melcher, subsequently, examined the electrodynamic charge relaxation at interfaces in a field applied normal to the interface.[6] Experiments using ac and dc fields indicated that conductance from charge convection at the interface played a role in destabilizing the interface. Saville has extensively investigated the electrohydrodynamic deformation of colloidal dispersions in weakly conducting liquids under static and oscillatory fields.[7−12] Onuki theoretically treated instabilities at the interface between two immiscible, nonionic fluids.[13] More recently, Nagel and co-workers investigated the time evolution of instabilities at liquid interfaces driven by an electric field applied normal to the interface.[14]

As discussed by Schäffer et al.[15,16] electrostatic forces across the surface of a polymer above its glass transition temperature will amplify surface waves resulting in a laterally ordered array of columns of the polymer spanning the gap between the electrodes. Their calculations indicated that the instability exhibits a well-defined lateral wavelength that follows a power-law dependence on the applied electric field, in agreement with theory.[15,16] Observations similar to those of Schäffer et al. were made by Chou and co-workers[17,18] with no applied external electric field. The more general case of a liquid/liquid bilayer confined between two solid electrodes was discussed by Lin et al.[19] Model calculations showed a means by which the amplification of fluctuations at an interface can be used to tune the size scale of self-assembled structures from the micron to the submicrometer level.

Here, a systematic characterization of structure formation at the interface of liquid/liquid bilayers in the electric field is reported. Regardless of the polymers used, very good agreement over many orders of magnitude in reduced wavelength and field strength is observed using no adjustable parameters. Routes toward even smaller size-scale structures are discussed.

Experimental Section

Materials. Poly(4-bromo styrene) (PSBr) (MW = 6.5×10^4) and poly(dimethylsiloxane) (PDMS) (200 Fluid, with a viscosity η = 10 000 cSt) were purchased from Aldrich Chemical Co. Polystyrene (PS) and poly(methyl methacrylate) (PMMA) were purchased from Polymer Laboratories Ltd. The molecular weight of PMMA and PS were PMMA-27K, MW = 2.7×10^4 (PDI = 1.04), PS-30.3 K, MW = 3.03×10^4 (PDI = 1.02) and PS-96 K, MW = 9.6×10^4 (PDI = 1.04). Deuterated polystyrene (dPS) with a molecular weight of 99.9K (PDI = 1.017) was synthesized in our laboratory by anionic polymerization. Indium−tin−oxide (ITO) microscope slides, a transparent electrode used in this study, were purchased from Delta Technologies ($25 \times 50 \times 1.1$ mm^3, $R_s \leq 100$ Ω).

Sample Preparation. In one study, a film of PS (MW = 30.3K), 550 nm in thickness, was spin-coated onto a freshly cleaned Si substrate. A layer of PDMS was then spin-coated directly on top of the PS film from a heptane solution to form

† Current address: Conti Tech, Gmbtt, GmbH, Hannover, Germany.

10.1021/ma0122425 CCC: $22.00
Published on Web 04/04/2002

Table 1. Characteristics of the Polymers

polymers	PDMS	PS	PMMA	PSBr	dPS
MW[a] (g/mol)	$\eta = 10\,000$ cSt	30 300/96 000	27 000	65 000	99 900
γ_{12} or γ[b] (mN/m)	$\gamma_{PDMS/PS} = 6.1$		$\gamma_{PS/PMMA} = 1.2$	39	33
	$\gamma_{PDMS/PMMA} = 3.8$		$\gamma_{PDMS/PMMA} = 3.8$		
ϵ[c]	2.46	2.95	5.24	4.09	2.95
n[d]	1.406	1.591	1.490	1.784	1.591
T_g[e] (°C)	−127	100	105	120	100

[a] Molecular weight. [b] Interfacial tension γ_{12} or surface tension γ at 170 °C.[20] [c] Dielectric constants at 170 °C.[24] [d] Refractive index. [e] Glass transition temperature.

a bilayer. Heptane is a nonsolvent for PS. Two bilayers with overall thicknesses 1.12 and 1.25 μm were prepared. In a second bilayer experiment, a 730 nm thick PS (MW = 96K) film was spin-coated from toluene solution on a cleaned Si wafer. A 290 nm thick film of PMMA (MW = 27K) was spin-coated on top of the PS film from an acetic acid solution where acetic acid is a nonsolvent for PS. Experiments were also performed on PMMA/PDMS bilayers. A thin layer of PMMA (MW = 27K) film was spin-coated from a toluene solution onto a Si wafer. A PDMS film was spin-coated from a heptane solution onto the PMMA layer, where heptane is a nonsolvent for PMMA, to form the PMMA/PDMS bilayer. The thickness of the PMMA and PDMS ranged from 180 to 290 nm and from 690 to 1030 nm, respectively.

Rails of silicon oxide were evaporated on the top of ITO-coated microscope slides. These were then placed on the top of the bilayers. The bilayers were annealed at 170 °C under N_2 for a day under an applied electric field and quenched to room temperature before removing the applied field.

To examine the polymer/polymer interface, the upper layer was removed with either heptane, in the case of PDMS, or acetic acid, in the case of PMMA. Residual heptane was removed by placing the sample under vacuum. Residual acetic acid was removed by thorough rinsing with deionized water and drying under vacuum at room temperature.

All film thicknesses were measured with a Rudolph Research AutoEL-II ellipsometer using a helium−neon laser (λ = 632.8 nm) at a 70° incidence angle. The dielectric constants of the solid polymers used in this study (PS, PMMA, and PSBr) were measured on melt-pressed 1.9 cm diameter, 1 mm thick disks, using a Novocontro dielectric spectrometer. The solid polymers were confined between two electrodes in a closed chamber under N_2. The dielectric constant of PDMS was measured using the BDS 1200 liquid sample cell. The dielectric measurements were performed at 5 Hz from 0 to 180 °C. The dielectric constants of all the polymers at 170 °C used in this study are given in Table 1. An Olympus BX60 optical microscope in the reflection mode was used to investigate the formation of structures at the interface between the two polymers. Atomic force microscopy (AFM) studies were performed with a Digital Instrument D3100 scanning force microscope in the tapping mode. Silicon nitride tips on cantilevers (Nanoprobe) with spring constants ranging from 29.3 to 63.9 N/m were used.

Results and Discussion

An optical micrograph of the PS/PDMS bilayer after 1 day under a 50V is shown in Figure 1a. Columns of PS through the upper PDMS layer are evident in the micrograph. Sine the refractive indices of PS and PDMS are 1.591 and 1.406, respectively, the contrast is rather weak. Nonetheless, the formation of the cylindrical structures at the interface is clearly seen. A 2D fast Fourier transform (FFT) of the optical micrograph is shown in the inset. The appearance of a ring in the transform indicates that there is a well-defined center-to-center distance between adjacent PS columns of 13.0 μm. From the micrograph the distribution of the center-to-center distances of adjacent columns was determined and is shown in Figure 1b. As seen, the average separation distance is 12.9 μm with a full width at half-maximum (fwhm) of 1.86 μm. The average diameter of the PS columns determined from the optical micrograph is 8.6 ± 0.5 μm.

After removing the upper PDMS layer with heptane, AFM was used to examine the surface of the underlying PS layer, i.e., the interface between the PDMS and PS layers. Shown in Figure 1c is the AFM image of the PS surface obtained in the height mode. As seen, columns of PS have been produced by the electrostatic pressure acting on the original PDMS/PS interface. The average size of the columns is 8.5 ± 0.3 μm with an average center-to-center distance between adjacent PS columns of 13.0 ± 1.0 μm. Shown in the inset is a 2D FFT of the AFM image. The six spots evident in these data indicate that, locally, there is a hexagonal symmetry in the lateral arrangement of the columns.

The electrohydrodynamic instability at the interface between two polymers under an applied voltage U across two electrodes separated by a distance d causes an amplification of fluctuations of a characteristic wavelength λ. The wavelength is given by[19]

$$\lambda = \frac{2\pi}{U\left|\frac{1}{\epsilon_2} - \frac{1}{\epsilon_1}\right|}\left(\frac{\gamma_{12}}{\epsilon_0}\right)^{1/2}\left(\frac{d - h_0}{\epsilon_1} + \frac{h_0}{\epsilon_2}\right)^{3/2} \qquad (1)$$

where $d - h$ and h are the film thicknesses of polymer 1 and polymer 2 with dielectric constants ϵ_1 and ϵ_2, respectively. γ_{12} is the interfacial tension between polymer 1 and 2, and ϵ_0 is the dielectric permittivity in a vacuum. By replacing γ_{12} with γ, the surface energy, ϵ_1 with 1, the dielectric constant of the air, and ϵ_2 with ϵ, eq 1 reduces to the case of a film confined between two electrodes with an air gap between the film and the upper electrode. This case was described previously by Schäffer et al.[15,16] Consequently, eq 1 applies to both the single and bilayer cases. Substituting the relevant parameters for the PDMS/PS bilayer case into eq 1 yields a characteristic distance of 15.8 μm, which agrees well with the 12.9 μm value measured experimentally.

In a second set of experiments, the upper PDMS layer was replaced by a PMMA layer to form PS/PMMA bilayer. Since the interfacial tension between PS and PMMA ($\gamma_{PS/PMMA}$ = 1.2 mN/m at 170 °C) is smaller than that for a PS/PDMS bilayer, ($\gamma_{PS/PDMS}$ = 6.1 mN/m) at any given temperature,[20] then, from eq 1, it would be expected that the characteristic wavelength λ would decrease. Shown in Figure 2a is the optical micrograph of the PS/PMMA bilayer after 1 day at 170 °C with 30 V applied after selectively removing the upper PMMA layer. Direct images of the bilayer without removal of the upper layer were not easily seen, since the refractive indices of PS and PMMA, 1.591 and 1.49, respectively, are very similar. The 2D FFT shown in the inset exhibits a ring, indicative of a well-defined separation

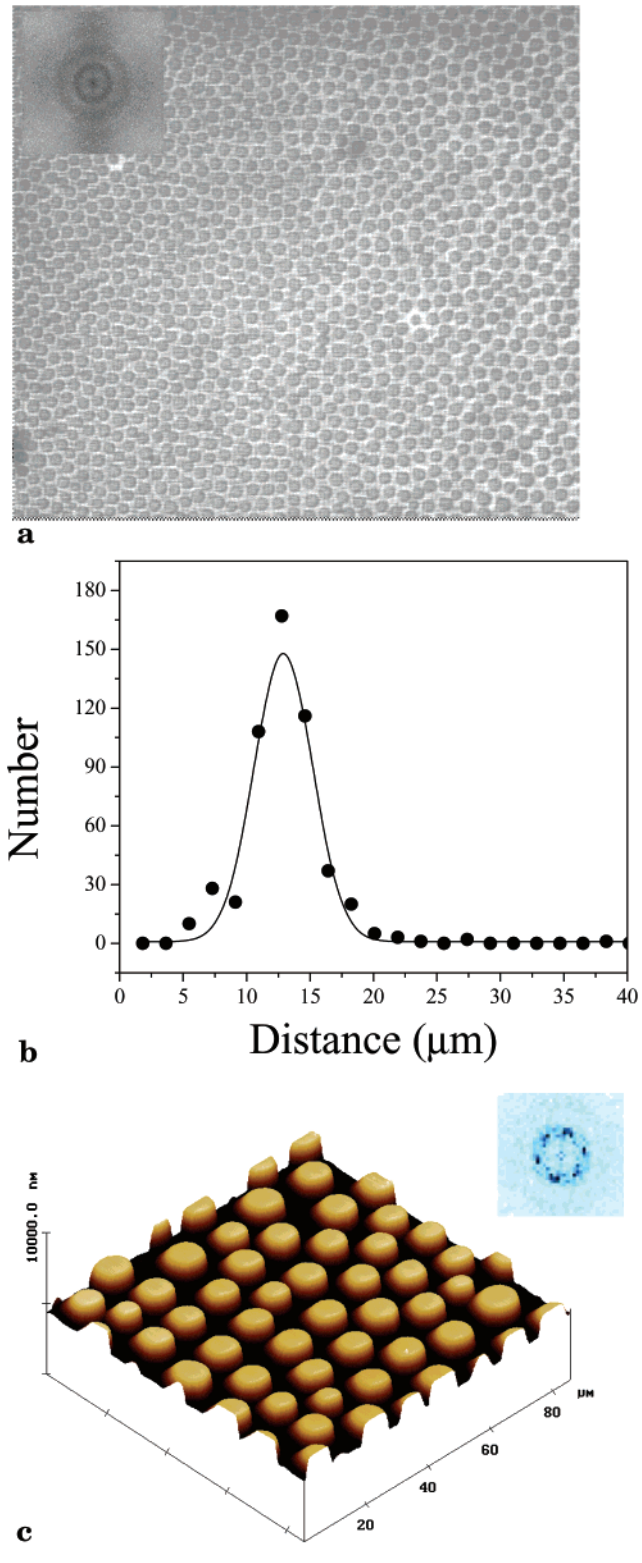

Figure 1. (a) Optical micrograph of a PS (h_{PS} = 550 nm)/PDMS (h_{PDMS} = 700 nm) bilayer exposed to 50 V at 170 °C for 1 day. The image size is 438 × 398 μm^2. The original color images were auto leveled and contrasted, and then converted to a gray scale to enhance the weak contrast due to the small refractive index difference between PS and PDMS. The inset shows the 2D fast Fourier transform (FFT) pattern of the corresponding optical micrographs. (b) Distribution function of the center-to-center distance between adjacent columns. (c) 3D AFM height image of the PS/PDMS bialyer after removal of the upper PDMS layer with heptane. The 2D FFT of the AFM image is shown in the inset.

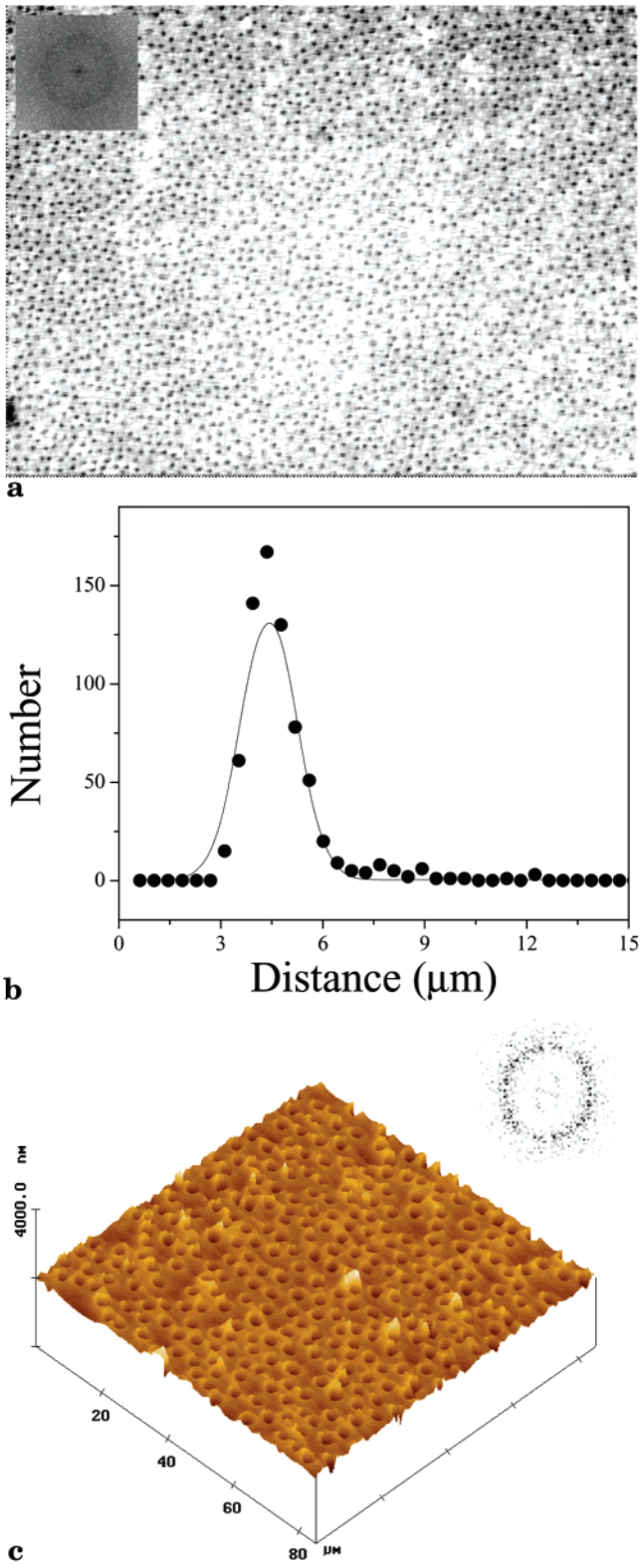

Figure 2. (a) Optical microscope image of PS/PMMA bilayer after removing the upper PMMA layer with acetic acid. The bilayer system held under 30 V at 170 °C for 1 day. The image size is 266 × 199 μm^2. The initial film thickness of PS and PMMA were 730 and 290 nm, respectively. The inset shows the 2D fast Fourier transform (FFT) pattern of the corresponding optical micrographs. (b) Distribution function of the center-to-center distance between adjacent columns. (c) AFM height image of the bilayer after removal of the upper PMMA layer. The 2D FFT of the AFM image is shown in the inset.

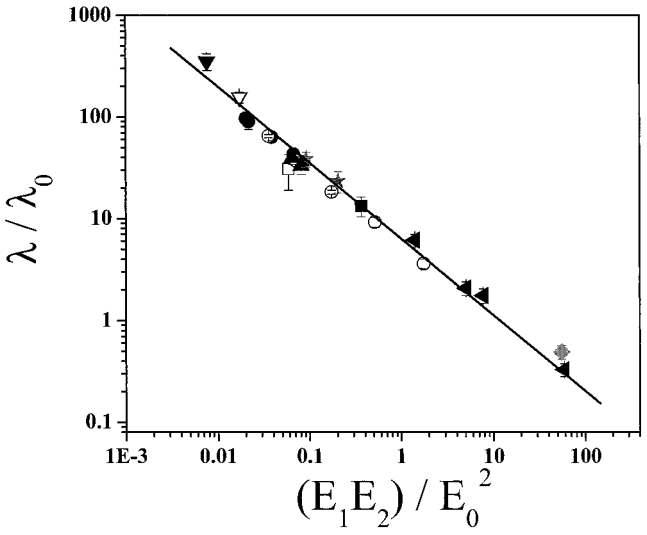

Figure 3. Master curve of the typical distance λ in varieties of thin film and bilayer experiments as a function of the electric field strength in layer 1 and layer 2. The different symbols corresponded to 10 data sets: (◆) PS/PMMA bilayer with h_{PS} = 730 nm; $(d - h_{PS})_{PMMA}$ = 290 nm, U = 30 V; (▼) PMMA/PDMS bilayer with h_{PMMA} = 180−290 nm, $(d - h_{PMMA})_{PDMS}$ = 690−1030 nm, U = 19−50 V; (★) PS/PDMS bilayer with h_{PS} = 305 nm, $(d - h_{PS})_{PDMS}$ = 400 nm and 720 nm respectively, U = 50 V; (▲) PS/PDMS bilayer with h_{PS} = 550 nm, $(d - h_{PS})_{PDMS}$ = 570 nm and 700 nm respectively, U = 50 V; (○) PSBr/air single layer with h_{PSBr} = 740 nm, d = 1.66−1.98 μm, U = 20−60 V; (●) dPS/air single layer with h_{dPS} = 530 nm, d = 1.06−1.85 μm, U = 30 V. ▼, ▽, ■, and □ were the measurements from ref 19, which corresponded to PI/air thin film, PI/ODMS bilayer, OS/air thin film, and OS/ODMS bilayer systems, respectively. The straight line was calculated based on eq 4 with a slope of $-3/4$.

distance between the features at the interfaces. Analysis of the optical micrograph yields an average diameter of the columns of 1.7 ± 0.3 μm. The distribution of the center-to-center distance between the columns, shown in Figure 2b, exhibits a maximum at 4.0 μm with a fwhm of 0.7 μm. Shown in Figure 2c is an AFM height image after removal of the PMMA layer by rinsing with acetic acid. Rather than columns, however, the AFM image shows that the features are holes penetrating through the PS film. This results, primarily, from the thickness of the individual layers. Here, the underlying PS layer was much thicker than the PMMA overlayer. Consequently, in this case, PMMA columns form within the PS layer. From eq 1, λ = 2.8 μm which is in good agreement with the value determined experimentally.

Experiments on PMMA/PDMS bilayers showed essentially the same behavior as that of the PS/PDMS bilayers. The film thickness of underlying PMMA layer was much thinner than that of the upper PDMS layer, therefore the PMMA columns were obtained. It should be pointed out that since the refractive index difference between PMMA and PDMS is quite small, ~0.08, the cylindrical structures at the PMMA/PDMS interface were barely visible with an optical microscope. After removing the PDMS layer with heptane, both optical microscopy and AFM were used to characterize the surface of the underlying PMMA. While numerous experiments were done on this bilayer, results from one experiment will be cited. This bilayer, under 19 V for 1 day, an average column diameter of 3.0 μm was found with and average center-to-center distance of 10.5 μm.

The characteristic wavelength, λ, of fluctuations at the interface that are amplified by the applied electric field depends on the sample geometry, the applied field and the dielectric constants of the materials. These parameters are explicitly shown in eq 1. We can define a reference wavelength and electric field as

$$\lambda_0 = \frac{\epsilon_0 U^2 (\epsilon_1 - \epsilon_2)^2}{\gamma_{12} (\epsilon_1 \epsilon_2)^{1/2}} \tag{2}$$

and

$$E_0 = \frac{U}{\lambda_0} \tag{3}$$

Using these we can define a reduced wavelength and field by dividing λ and E by λ_0 and E_0, respectively. For the reduced wavelength we have

$$\frac{\lambda}{\lambda_0} = 2\pi \left(\frac{E_1 E_2}{E_0^{\,2}} \right)^{-3/4} \tag{4}$$

where E_1 and E_2 are the electric field strengths in layer 1 and 2, respectively. By replacing ϵ_1 with 1.0 and E_2 with E_P, the dimensionless variables, this can be reduced to the polymer thin film case investigated by Schäffer et al.[15,16]

A master curve where the reduced wavelength λ/λ_0 is plotted as a function of the reduced field strength E_1E_2/E_0^2 is shown in Figure 3. Shown are experimental data obtained from different experiments where the geometry of the system, the field strengths and the polymers have been varied. In addition, data from previous experiments on single polymer layers are included. The solid line in the figure is the theoretical reduced wavelength as a function of the reduced field strength using no adjustable parameters. As can be seen, there is excellent agreement between experiment and theory over 4 orders of magnitude in the reduced wavelength and reduced field strength.

The derivation of eq 1 uses a linear approximation in treating the amplitude of fluctuations at the interface. Consequently, eq 1 should only be valid at the early stages of fluctuation growth and not, necessarily, at the latter stages of the process which includes the results shown here. Shown in Figure 4 are a series of AFM height images characterizing the development of structure at the interface of a PMMA/PDMS bilayer with 19 V applied at 170 °C at different times. Each of the images was obtained on different bilayer samples where the upper PDMS layer was removed with heptane. Figure 4a shows that the initial interface was featureless. With time, fluctuations having a well-defined lateral wavelength are seen to emerge (Figure 4b). The 2D FFT of this image, shown in the inset, exhibits a maximum characteristic of a wavelength or average center-to-center distance of 10.5 μm. As time progresses, the amplitude of the fluctuations increases, the fluctuations become sharper and well-defined and begin to show a lateral order, and instabilities that give rise to the formation of columns appear (Figure 4c). The 2D FFT of this AFM image, shown in the inset, exhibits a maximum corresponding to an average center-to-center distance of 10.5 μm, the same spacing seen at earlier times. The surface of the PMMA after the formation of PMMA columns that extend to the upper electrode is shown in

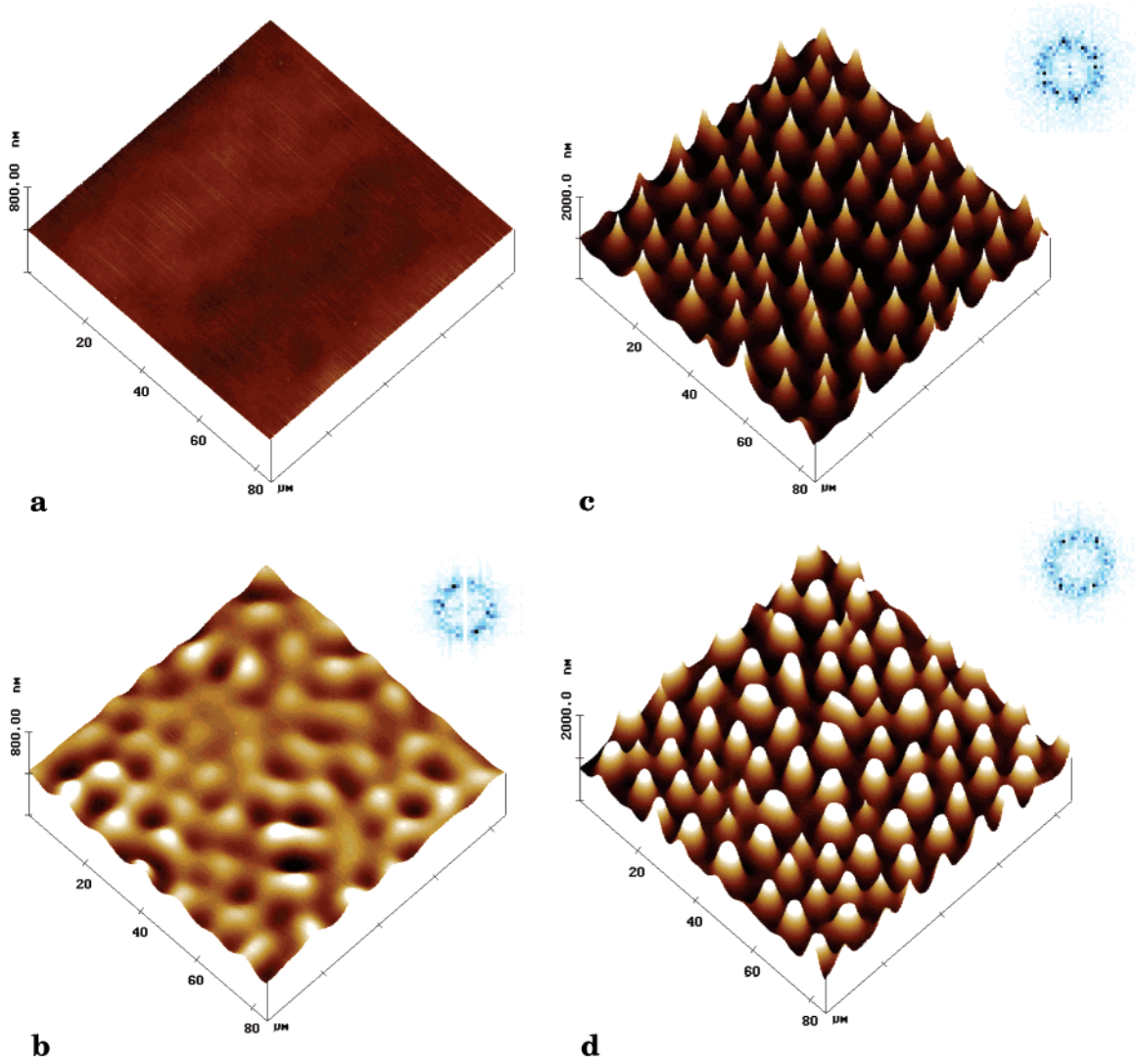

Figure 4. Series of AFM height images as a function of time of a PMMA/PDMS bilayer after removal of the PDMS layer (h_{PMMA} = 220 nm, h_{PDMS} = 890 nm) with 19 V applied with heptane. The insets show a FFT of the images. The time sequence of the images correspond to the (a) initial interface, (b) initial stages of fluctuation growth, (c) amplification of fluctuations, and (d) the impingement of PMMA columns on the upper electrode.

Figure 4d. Contact with the upper electrode is evidenced by the flattened top of the columns and a well-defined lateral ordering is evident. The 2D FFT shown in the inset exhibits a maximum corresponding to a center-to-center distance between adjacent columns of 10.5 μm, the same as that seen at earlier times. The preservation of the characteristic distance throughout the growth of the columns justifies the comparison of the results obtained at later times to the linearized theoretical predictions. However, this does not hold true for the characteristic times describing the kinetic growth of these structures. As discussed earlier, discrepancies between the predicted times and those observed, based on the late stages of growth, are seen due to our inability to characterize the kinetics of the growth quantitatively.[19] These studies are currently in progress using fluorescent confocal microscopy and will be discussed later.

The quantitative agreement between experiment and theoretical predictions in the master curve of Figure 3 shows that by control of the sample geometry, the applied field or the interfacial energy, the size scale of the fluctuations can be controlled or manipulated. For a given geometry, polymer pair, and field strength, reducing the interfacial tension provides a route to decrease the size scale of the fluctuations. Smaller size scale fluctuations that produce a larger interfacial area, can be amplified if the interfacial tension is reduced. It is well-known that the addition of block copolymers that segregate to the polymer/polymer interfaces reduces the interfacial tension and, hence, provides an easy route toward structures that are hundreds to tens of nanometers in size.[21−23] In the case of thin polymer films, a surface active agent should cause a similar effect. With fixed interfacial energies, increasing the electric field provides the easiest route to control the lateral length scales of the fluctuations. By combination of both these effects, the characteristic lateral length scale of the fluctuations can easily be placed on the nanoscopic level. If the relative thicknesses of the two layers are changed, either columns or holes can be produced that have lateral length scales defined by the linearized theoretical arguments. Finally, it should be pointed out that polymers offer a unique advantage over low molar mass fluids, since the structures produced by the applied field can be frozen-in by quenching below the glass transition temperature.

Conclusions

An electric field applied normal to polymer interface was shown to enhance fluctuations which, eventually, led to the growth of columnar structures. A linearized theory developed previously was shown to be applicable to a wide range of simple polymer films and polymer/polymer interfaces. A master curve, using no adjustable parameters, was shown to describe the results from a wide range of systems over many orders of magnitude in reduced field strength and distance. The applicability of the linearized theory to describe the lateral length scales of the fluctuations from the early stages of amplification to the formation of columnar structures was shown. Clear routes have been shown by which the size scale of the structures can be manipulated over many lengths scales ranging from the microscopic to the nanoscopic.

Acknowledgment. This work was funded by NASA under Contract NAG8-694, the National Science Foundation supported Materials Research Science and Engineering Center at the University of Massachusetts (DMR98-09365), the Northeastern Environmental Technology Institute and the Department of Energy, Office of Energy Sciences (DE-FG-96ER45612), and the Dutch Stichtung voor Fundamenteel on der Zoek der Materie.

Note Added after ASAP Posting

This article was released ASAP on 4/4/02 with a few minor differences. The correct version was posted on 4/5/02.

References and Notes

(1) Swan, J. W. *Proc. R. Soc. London* **1897**, *62*, 38.
(2) Glenn, W. E. *J. Appl. Phys.* **1959**, *30*, 1870.
(3) Cressman, P. J. *J. Appl. Phys.* **1963**, *34*, 2327.
(4) Killat, U. *J. Appl. Phys.* **1975**, *46*, 5169.
(5) Reynolds, J. M. *Phys. Fluids* **1965**, *8*, 161.
(6) Melcher, J. R.; Smith, C. V. *Phys. Fluids* **1969**, *12*, 778.
(7) Vizika, O.; Saville, D. A. *J. Fluid Mech.* **1992**, *239*, 1.
(8) Saville, D. A. *Colloids Surf. A* **1994**, *92*, 29.
(9) Trau, M.; Sankaran, S.; Saville, D. A.; Aksay, T. A. *Nature (London)* **1995**, *374*, 437.
(10) Trau, M.; Sankaran, S.; Saville, D. A.; Aksay, T. A. *Langmuir* **1995**, *11*, 4665.
(11) Saville, D. A. *Annu. Rev. Fluid Mech.* **1997**, *29*, 27.
(12) Anklam, M. R.; Saville, D. A.; Prud'homme, R. K. *Colloid Polym. Sci.* **1999**, *277*, 957.
(13) Onuki, A. *Physica A* **1995**, *217*, 38.
(14) Oddershede, L.; Nagel, S. R. *Phys. Rev. Lett.* **2000**, *85*, 1234.
(15) Schäffer, E.; Thurn-Albrecht, T.; Russell, T. P.; Steiner, U. *Nature (London)* **2000**, *403*, 874.
(16) Schäffer, E.; Thurn-Albrecht, T.; Russell, T. P.; Steiner, U. *Europhys. Lett.* **2001**, *53*, 518.
(17) Chou, S. Y.; Zhuang, L.; Guo, L. *Appl. Phys. Lett.* **1999**, *75*, 1004.
(18) Chou, S. Y.; Zhuang, L. *J. Vac. Sci. Technol. B* **1999**, *17*, 3197.
(19) Lin, Z.; Kerle, T.; Baker, S. M.; Hoagland, D. A.; Schaffer, E.; Steiner, U.; Russell, T. P. *J. Chem. Phys.* **2001**, *114*, 2377.
(20) Wu, S. *Polymer Interface and Adhesion*; Marcel Dekker: New York, 1982.
(21) Kohler, J.; Riess, G.; Banderet, A. *Eur. Polym. J.* **1968**, *173*, 187.
(22) Anastasiadis, S. H.; Gancarz, I.; Koberstein, J. T. *Macromolecules* **1989**, *22*, 1449.
(23) Budkowski, A.; Klein, J.; Steiner, U.; Fetters, L. J. *Macromolecules* **1993**, *26*, 2470.
(24) The dielectric constant of PMMA at 170 °C was found to be 5.3 in the measurement by Mazur,[25] which is consistent with our measurement.
(25) Mazur, K. *J. Phys. D. Appl. Phys.* **1997**, *30*, 1383.

MA0122425